nature immunology

ATP11C is critical for the internalization of phosphatidylserine and differentiation of B lymphocytes

Mehmet Yabas[1], Charis E Teh[1], Sandra Frankenreiter[1], Dennis Lal[1], Carla M Roots[2], Belinda Whittle[3], Daniel T Andrews[2], Yafei Zhang[3], Narci C Teoh[4], Jonathan Sprent[5], Lina E Tze[2], Edyta M Kucharska[1], Jennifer Kofler[2], Geoffrey C Farell[4], Stefan Bröer[6], Christopher C Goodnow[2,7] & Anselm Enders[1,7]

Subcompartments of the plasma membrane are believed to be critical for lymphocyte responses, but few genetic tools are available to test their function. Here we describe a previously unknown X-linked B cell–deficiency syndrome in mice caused by mutations in *Atp11c*, which encodes a member of the P4 ATPase family thought to serve as 'flippases' that concentrate aminophospholipids in the cytoplasmic leaflet of cell membranes. Defective ATP11C resulted in a lower rate of phosphatidylserine translocation in pro-B cells and much lower pre-B cell and B cell numbers despite expression of pre-rearranged immunoglobulin transgenes or enforced expression of the prosurvival protein Bcl-2 to prevent apoptosis and abolished pre-B cell population expansion in response to a transgene encoding interleukin 7. The only other abnormalities we noted were anemia, hyperbilirubinemia and hepatocellular carcinoma. Our results identify an intimate connection between phospholipid transport and B lymphocyte function.

The differentiation of B lymphocytes from hematopoietic stem cells is one of the best-defined cell-differentiation processes in vertebrates. Its analysis by molecular genetics has elucidated fundamental mechanisms for normal immunity, human immunodeficiency diseases, DNA transcription, rearrangement and repair, cell signaling and cancer. B cell differentiation is now viewed as proceeding in a graded manner, guided by a complex, self-reinforcing network of B cell–specific transcriptional regulators and receptor signaling systems[1–4]. Understanding how the elements of this network are integrated has only begun and hinges on the identification of essential missing steps.

The stepwise differentiation of B cells is demarcated by the expression of different cell surface and intracellular proteins[5–7]. Cells of the earliest B lineage–biased stage, B lymphoid progenitors, express the α-chain of the interleukin 7 receptor (IL-7Rα; CD127), abundant CD43, and Ly6D. These are succeeded by pre-pro-B cells (fraction A cells), which retain those markers but also express B220, and then by pro-B cells (fraction B), which acquire intermediate expression of CD24 (heat-stable antigen) and CD19. Development to the pro-B cell stage and beyond requires a feed-forward network of interactions among IL-7 produced by nearby stromal cells, IL-7R signaling activating the transcription factor STAT5, and the B lineage–specific transcription factors PU.1, EBF-1, E2A and Pax5 (refs. 1,3,4,8). Differentiation to the pro-B cell stage enables recombination of variable (V), diversity (D) and joining (J) elements in the immunoglobulin heavy chain gene, which results in the synthesis of cytoplasmic immunoglobulin M (IgM; cμ) heavy chains that assemble with surrogate light chains and CD79α and CD79β proteins into a pre–B cell antigen receptor (pre-BCR)[9]. Expression of the pre-BCR intracellularly ($c\mu^+$) defines a pre-B cell, enhances the growth response to IL-7 (refs. 10,11) and signals a further increase in CD24, induction of the cytokine receptor CD25 and downregulation of the leukosialin CD43. Pre-B cells switch to light-chain gene rearrangement; this results in the assembly of complete IgM molecules with CD79α and CD79β, which are expressed as BCRs on the cell surface, and these cells progressively lose IL-7Rα expression. Although B cell differentiation depends on integrated signaling by the pre-BCR and IL-7R, much remains to be understood about the initiation of and crosstalk between these processes.

A growing body of work suggests that many immunological and cell biological signaling events hinge on organization of the plasma membrane into specialized substructures, such as the lateral concentration of particular lipids into rafts or the asymmetrical concentration of specific phospholipids between the exoplasmic and cytoplasmic leaflets[12,13]. Exploring the function of these membrane specializations in lymphocytes has been limited by the paucity of genetic tools for specific testing of their function *in vivo*, and most experiments have depended on disruptive approaches using detergents and biochemical fractionation. Phosphatidylserine (PS) is an abundant aminophospholipid normally concentrated almost exclusively in the cytoplasmic leaflet[13], where it seems to be important for membrane budding and the formation of clathrin-coated vesicles during post-Golgi transport

[1]Ramaciotti Immunization Genomics Laboratory, Department of Immunology, The John Curtin School of Medical Research, The Australian National University, Canberra, Australia. [2]Department of Immunology, The John Curtin School of Medical Research, The Australian National University, Canberra, Australia. [3]Australian Phenomics Facility, The John Curtin School of Medical Research, The Australian National University, Canberra, Australia. [4]Gastroenterology and Hepatology Unit, Australian National University Medical School, The Canberra Hospital, Canberra, Australia. [5]Immunology Program, Garvan Institute of Medical Research, Darlinghurst, Australia, and World Class University–Integrative Biosciences and Biotechnology Program, Pohang University of Science and Technology, Pohang, Korea. [6]Division of Biomedical Science and Biochemistry, Research School of Biology, The Australian National University, Canberra, Australia. [7]These authors contributed equally to this work. Correspondence should be addressed to C.C.G. (chris.goodnow@anu.edu.au) or A.E. (anselm.enders@anu.edu.au).

Received 8 November 2010; accepted 21 February 2011; published online 20 March 2011; doi:10.1038/ni.2011

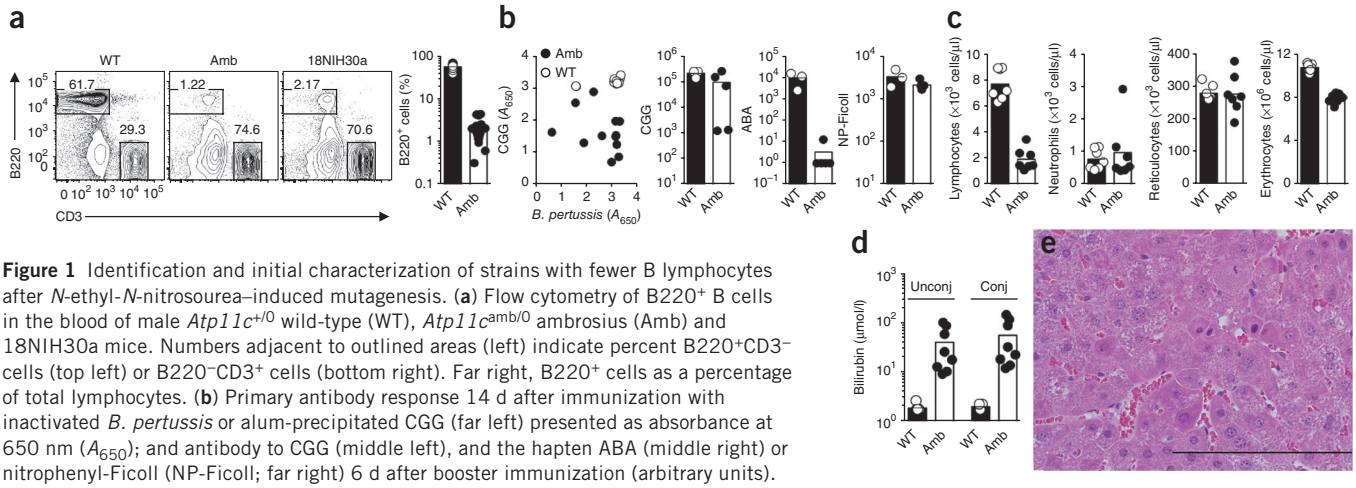

Figure 1 Identification and initial characterization of strains with fewer B lymphocytes after *N*-ethyl-*N*-nitrosourea–induced mutagenesis. (**a**) Flow cytometry of B220$^+$ B cells in the blood of male *Atp11c*$^{+/0}$ wild-type (WT), *Atp11c*$^{amb/0}$ ambrosius (Amb) and 18NIH30a mice. Numbers adjacent to outlined areas (left) indicate percent B220$^+$CD3$^-$ cells (top left) or B220$^-$CD3$^+$ cells (bottom right). Far right, B220$^+$ cells as a percentage of total lymphocytes. (**b**) Primary antibody response 14 d after immunization with inactivated *B. pertussis* or alum-precipitated CGG (far left) presented as absorbance at 650 nm (A_{650}); and antibody to CGG (middle left), and the hapten ABA (middle right) or nitrophenyl-Ficoll (NP-Ficoll; far right) 6 d after booster immunization (arbitrary units). (**c**) Lymphocytes, neutrophils, reticulocytes and erythrocytes in the blood of *Atp11c*$^{amb/0}$ mice and their *Atp11c*$^{+/0}$ littermates. (**d**) Unconjugated (Uconj) and conjugated (Conj) bilirubin in the plasma of *Atp11c*$^{+/0}$ and *Atp11c*$^{amb/0}$ mice. (**e**) Typical dysplastic focus on a hematoxylin and eosin–stained liver section from an *Atp11c*$^{amb/0}$ mouse at 6 months. Scale bar, 200 μm. Each symbol (**a**–**d**) represents a single mouse. Data are from more than five experiments (**a**) or are representative of two experiments (**b**–**d**) or one experiment (**e**) with four to ten mice per group in each.

and endocytosis, on the basis of studies in yeast[14]. PS in the cytoplasmic leaflet also activates protein kinase C-β and provides a docking site for a range of other signaling proteins[15]. During the early stages of cell death and during certain forms of cell activation, such as platelet activation, PS redistributes to the exoplasmic leaflet, where it can be recognized by specific PS receptors or blood proteins such as clotting factor VIII (ref. 13). Binding of fluorescent annexin V to PS in the exoplasmic leaflet is widely used experimentally for measurement of the initiation of apoptosis. Macrophages bear receptors that recognize exoplasmic PS as 'eat-me' signals[16,17]. Viable cells also display PS during certain conditions independently of apoptosis—notably, pre-B cells that have received pre-BCR signals, marginal zone B cells[18] and some B cell lymphomas[19]—but the cause and function of exoplasmic PS in these circumstances is obscure.

Phospholipids such as PS 'flip-flop' very slowly between the inner and outer membrane leaflets in protein-free membranes, with a half-time of hours or days[20]. Asymmetry of the plasma membrane is actively generated by two groups of ATP-dependent transporters. ABC-type transporters ('floppases') are responsible for the active transport of specific lipids to the exoplasmic leaflet[20]. 'Flipping' of PS and other aminophospholipids into the inner leaflet against their concentration gradient is greatly accelerated by phospholipid translocases ('flippases') thought to be members of the P4 ATPase family of ten-transmembrane-domain proteins[21–23]. The functions of the P4 ATPases have mostly been identified by genetic analysis of yeast[14], and the role of the 14 P4 ATPases in humans and other mammals is mostly unexplored. So far only one gene has clearly been linked to human disease; *ATP8B1* (also known as *FIC1*) is mutated in two forms of heritable intrahepatic cholestasis[24]. Here we show that a defect in ATP11C, a ubiquitously expressed P4 ATPase of previously unknown function, results in lower B cell PS flippase activity and disrupts B cell development and antibody production, and also causes hepatocellular carcinoma. Our findings demonstrate a critical role for membrane asymmetry in B lymphocytes and open the way to the study of its function in mammalian cells.

RESULTS

X-linked B cell deficiency and liver disease

Screening of C57BL/6 mouse pedigrees with *N*-ethyl-*N*-nitrosourea–induced mutations by flow cytometry identified two independent strains, ambrosius and 18NIH30a, with many male offspring having B cell frequencies in blood that were 3% that of controls (**Fig. 1a**). These mice nevertheless had normal frequencies of T cells and natural killer (NK) cells (data not shown). B cell deficiency was inherited as a Mendelian recessive, X-linked trait in successive generations. Immunization with inactivated *Bordetella pertussis* or alum-precipitated chicken γ-globulin (CGG) coupled to the hapten azo-benzene-arsonate (ABA) resulted in a variably lower primary antibody response to each antigen in the mutant mice (**Fig. 1b**, left). Booster immunization with ABA-CGG 6 weeks later again resulted in variably lower antibody responses to the CGG protein carrier, whereas antibodies to the ABA hapten (which depends on antibody hypermutation and selection in germinal centers) were almost completely absent from all mutant mice (**Fig. 1b**, middle). In contrast, the mutant mice made a normal IgM antibody response to the T cell–independent antigen nitrophenyl-Ficoll (**Fig. 1b**, right). Thus, the much lower number of circulating B cells caused a variable humoral immune deficiency.

The mutant mice were normal in appearance, size and weight, showed no discernable change in gait or behavior, and were fertile. The only other phenotypic abnormalities detected were fewer lymphocytes, normochromic anemia with 30% fewer total erythrocytes but normal reticulocyte numbers, and notably yellow plasma due to a 30-fold higher concentration of unconjugated and conjugated bilirubin (**Fig. 1c**,**d**). Other measures of liver injury, such as plasma alanine aminotransferase and aspartate aminotransferase, were similar in mutant and control mice (data not shown). However, necropsy showed gross and microscopic liver pathology consistent with hepatocellular carcinoma in all mutant mice (ten of ten) analyzed at 6 months of age and not in normal control mice. Liver tumors were well to poorly differentiated hepatocellular carcinomas containing areas of hemorrhage, necrosis and hypervascularity. Tumor development in these mice was probably preceded by the formation of foci of altered hepatocytes (**Fig. 1e** and **Supplementary Fig. 1**). Several such foci were present in the liver tissue surrounding the tumors, with many mitotic figures, many of which were multipolar with condensed and asymmetric chromatin aggregation (**Supplementary Fig. 1a**,**b**). Other dysplastic features included nuclear anisocytosis, hyperchromasia, pleomorphism and a higher nucleus/cytoplasm ratio (**Fig. 1e** and **Supplementary Fig. 1**). As there are few experimental mouse models

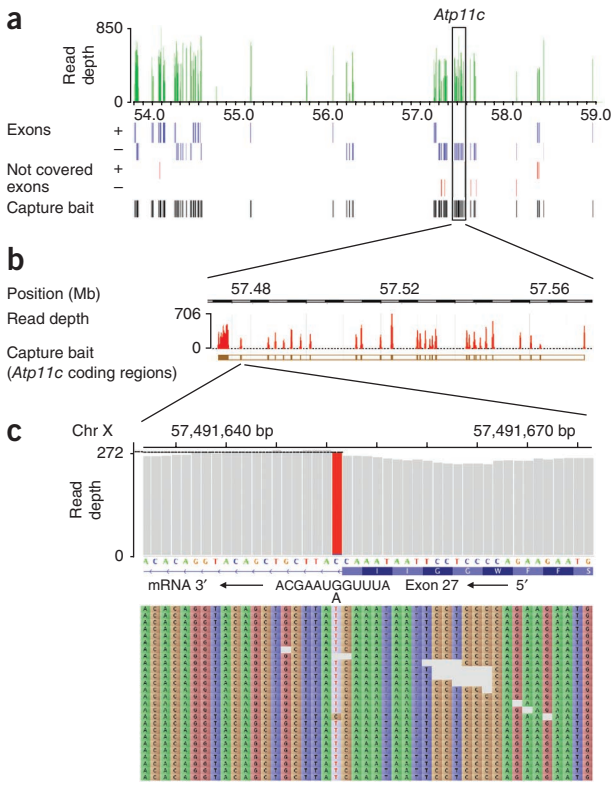

Figure 2 Identification of a splice-site mutation in *Atp11c* by next-generation DNA sequencing. (**a**) Read depth from a single sequencer lane across the tiled region between 54 and 59 megabases on the X chromosome; box outlines *Atp11c*. Below: blue lines, all annotated exons on the sense and antisense strands; red lines, exons with a read depth of less than 5; black lines, capture baits used for enrichment of exons from genomic DNA. (**b**) Enlargement of *Atp11c* outlined in **a**, with read depth and chromosomal coordinates (National Center for Biotechnology Information build 37.1). (**c**) *Atp11c* exon 27 splice donor at single-nucleotide resolution, read depth across these nucleotides and sequence of first 30 reads. Chr, chromosome; bp, base pairs. Data are representative of two independent experiments.

available for the study of hepatocellular carcinoma, the liver pathology of the mutant strain is of interest, but it will require detailed analysis beyond the scope of this study.

Identification of *Atp11c* mutations by next-generation sequencing

Linkage analysis of (C57BL/6 × CBA)F_2 offspring mapped the *ambrosius* mutation to an X-chromosomal region distal to marker rs13483763 at position 54,012,901 (National Center for Biotechnology Information build 37.1). To capture and sequence exons in this region annotated in the National Center for Biotechnology Information Reference Sequence database (RefSeq), we designed a custom-targeted DNA capture array, from which we prepared RNA 'baits' and hybridized those with fragmented genomic DNA from an ambrosius male (**Fig. 2a**). We sequenced the enriched DNA in paired-end mode for 100 cycles on a single lane of the sequencer. For the bait targets, the median read depth from a single lane of data was 138, and 96% of the nucleotides were covered with a read depth of 5 or greater. We obtained a median read depth of 137 across all RefSeq exons in the mutation-containing region and a read depth of 5 or greater for approximately 93% of the nucleotides in these exons. Capture and sequencing was done in replicate at two facilities and yielded highly reproducible results. These results demonstrate the utility of exon capture and next-generation DNA sequencing in accelerating mutation identification.

In the exons sequenced, we identified a single mutation ('amb') in both capture data sets that was confirmed by Sanger sequencing; this mutation was in a previously uncharacterized gene, *Atp11c*. It was a G-to-A substitution in the exon 27 splice donor sequence at position +1 of intron 27 (**Fig. 2b**,**c**). The normal G nucleotide at position +1 is invariant in 5′ splice donor sequences and its substitution would be predicted to abolish splicing, yielding either an in-frame UGA stop codon at the 3′ end of exon 27 (**Fig. 2c**) or aberrant use of alternative splice donors. PCR amplification of cDNA from mutant and wild-type bone marrow or spleen with primers located in exons 25 and 29 yielded a shorter product in the mutant mice (**Supplementary Fig. 2a**), identified by sequencing to skip exon 27 and splice exon 26 to exon 28. The resulting deletion of 104 base pairs introduced a frame shift after the amino acid at position 1010, which abolished the C-terminal residues that form the final two transmembrane domains and cytoplasmic tail of ATP11C protein, according to modeling along the structure of the rabbit sarcoplasmic-endoplasmic reticulum calcium ATPase 1 (**Supplementary Figs. 2b** and **3**). We identified an independent *Atp11c* mutation by Sanger sequencing in strain 18NIH30a that also disrupted an invariant, essential splice-donor nucleotide but in the preceding exon 26 splice-donor sequence (intronic T-to-G substitution at position +2: 5′-TCTGA**AGg*t*aga**ttttt to AACTCTGA**AGggtaga**ttttt-3′; where upper case indicates exonic sequence, lower case indicates intronic sequence, bolding indicates bases that are part of the splice-donor consensus sequence and italics indicate the mutated base). Given the severity of these mutations and the similarity of the phenotype of these mice to the phenotype caused by an *Atp11c* mutation reported in the accompanying study in this issue that results in truncation of almost half the protein[25], it is likely that these mutations fully inactivate the protein.

Smaller B cell subsets, except marginal zone B cells

The requirement for normal ATP11C in B cells was cell autonomous in chimeric mice reconstituted with an equal mixture of CD45.2$^+$ hemizygous (*Atp11c*$^{amb/0}$) bone marrow and CD45.1$^+$ wild-type (*Atp11c*$^{+/0}$) marrow, so that *Atp11c*$^{amb/0}$ B cells represented only 1% of B cells (**Supplementary Fig. 4**). In the same mixed chimeras, *Atp11c*$^{amb/0}$ T cells and NK cells nevertheless accumulated in proportions approximately equal to those in their wild-type counterparts, which established that there was little or no competitive disadvantage of mutant cells in T cells, NK cells or their hematopoietic progenitors.

Analysis of hematopoietic progenitors, including hematopoietic stem and progenitor cells, multipotent progenitors and common lymphoid progenitors, showed that the bone marrow of *Atp11c*$^{amb/0}$ mice had normal or slightly larger populations of these cells than their wild-type littermates had (**Supplementary Fig. 5a**,**b**). More detailed analysis of other lineages in the bone marrow showed that *Atp11c*$^{amb/0}$ mice had normal numbers of myeloid, erythroid and NK cells and slightly more T cells (**Supplementary Fig. 5c**,**d**), which indicated that ATP11C was not required for blood cell progenitors and their development into other lineages. We did a systematic analysis of B cell subsets in *Atp11c*$^{amb/0}$ and control mice to determine which stages of B cell development were disrupted. In the bone marrow, the absolute number of leukocytes was normal but the frequency and number of B cells were lower in *Atp11c*$^{amb/0}$ mice, at 15–18% of that in wild-type controls (**Fig. 3a–c** and **Table 1**). The number of CD43$^+$CD24^{int} pro-B cells was 60% of normal, whereas the numbers of CD43^{lo}CD24^{hi} pre-B cells and IgM$^+$IgD$^-$ immature B cells were

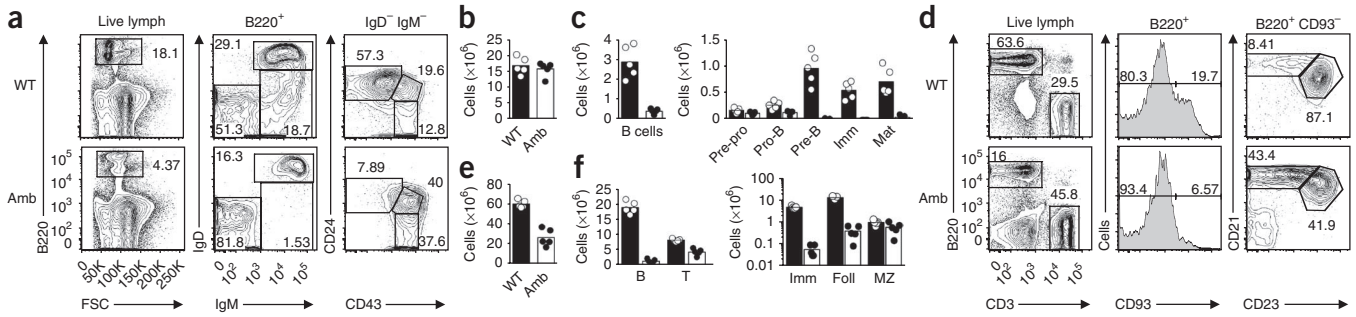

Figure 3 The *Atp11c*^{amb} mutation results in smaller B cell subsets except marginal zone B cells. (**a**) Flow cytometry of bone marrow cells from male *Atp11c*$^{+/0}$ and *Atp11c*$^{amb/0}$ mice. Numbers adjacent to outlined areas indicate percent B220$^+$ B cells (left column); IgD$^+$IgM$^+$ mature B cells (top right), IgD$^-$IgM$^+$ immature B cells (bottom right) and IgD$^-$IgM$^-$ pro- and pre-B cells (bottom left) in the B220$^+$ subset (middle column); and CD24^{hi}CD43$^-$ pre-B cells (top left), CD24^{int}CD43$^+$ pro-B cells (top right) and CD24$^-$CD43$^+$ pre-pro-B cells (bottom right) among cells gated on B220$^+$ IgM$^-$ IgD$^-$ cells (right column). FSC, forward scatter. (**b**,**c**) Leukocytes (**b**) and B cells and B cell subsets (**c**) in bone marrow from *Atp11c*$^{+/0}$ and *Atp11c*$^{amb/0}$ mice. Imm, immature; Mat, mature. (**d**) Flow cytometry of B cell subpopulations in spleens from male *Atp11c*$^{+/0}$ and *Atp11c*$^{amb/0}$ mice. Numbers adjacent to outlined areas indicate percent B220$^+$ B cells (top left) and CD3$^+$ T cells (bottom right; left column), or CD21^{hi}CD23$^-$ marginal zone B cells (left) and CD21^{int}CD23$^+$ follicular B cells (right) in the B220$^+$CD93$^-$ mature B cell subset (right column); and numbers above bracketed lines indicate percent CD93$^-$ mature B cells (left) and CD93$^+$ immature B cells (right) among B220-gated cells (middle column). (**e**,**f**) Leukocytes (**e**) and lymphocyte subsets (**f**) in the spleen. Each symbol (**b**,**c**,**e**,**f**) represents a single mouse (bars and symbols in **c**,**f** as in **b**,**e**). Data are representative of at least five independent experiments with two to five mice per group in each (mean and individual values in **b**,**c**,**e**,**f**).

only 6% and 1.8% of normal, respectively. IgM$^+$IgD$^+$ mature recirculating B cells in the bone marrow were 11% of normal numbers, and these had a much higher density of IgM than did those of their wild-type littermates (**Fig. 3a–c**). When we sorted bone marrow B cell progenitors negative for IgM at the membrane (mIgM) and for lineage markers by their expression of CD43, CD24 and BP-1, we found normal numbers of pre-pro-B cells (fraction A) in the mutant mice, but progressively fewer pro-B and pre-B cells in fractions B, C and C′ (**Supplementary Fig. 6**). These data establish that ATP11C is required for B cells to differentiate normally past the pro-B cell stage.

In the spleen, the number of B cells in *Atp11c*$^{amb/0}$ mice was also lower, at 9% of that in wild-type mice (**Fig. 3d–f** and **Table 1**). Consistent with the deficits in the bone marrow, immature B cells in the spleen were also less abundant, at 1% of the number in wild-type mice, and recirculating follicular B cells were 5% of the normal number. The follicular B cells were located normally, based on immunofluorescence staining of spleen sections (data not shown), but they had an abnormal surface phenotype of more IgM and CD21 and less CD23. In contrast, marginal zone B cells were present in normal numbers and had a normal surface phenotype in *Atp11c*$^{amb/0}$ mice (**Fig. 3d**,**f**) so that they made up approximately 40% of all splenic B cells. In the peritoneal cavity of *Atp11c*$^{amb/0}$ mice, the subsets of B-1a, B-1b and B-2 cells were smaller, at less than 10% of normal (**Supplementary Fig. 7**). These data indicate that marginal zone B cells are unique among B cell subsets by either not requiring ATP11C activity or being able to compensate for its loss.

ATP11C deficiency abolishes effects of an *Il7* transgene

The transition from pro-B cell to pre-B cell is dependent on signaling through IL-7R and successful rearrangement of immunoglobulin heavy-chain genes[10]. To determine if defects in these processes and subsequent apoptosis caused the developmental block in *Atp11c*$^{amb/0}$ mice, we crossed mice with that mutation with four other strains of mice: mice with transgenic expression of the gene encoding the pro-survival protein Bcl-2 driven by the promoter of the gene encoding the adaptor Vav (*Vav-Bcl2* mice), to inhibit apoptosis[26]; mice with transgenic expression of *Il7* driven by the E_α promoter of the gene encoding mouse major histocompatibility complex class II (*H2Ea-Il7* mice), which have much more IL-7 (ref. 27); or mice expressing the MD4 or SW_{HEL} transgene[28,29], which have immunoglobulin heavy- and light-chain genes already rearranged (**Fig. 4** and **Table 1**).

The number of pre-B cells in *Atp11c*$^{amb/0}$ *Vav-Bcl2* mice was 29% of the number in *Atp11c*$^{+/0}$ *Vav-Bcl2* control mice, which represented partial restoration relative to the number of pre-B cells in *Atp11c*$^{amb/0}$ mice without *Vav-Bcl2*, which was 6% of normal (**Fig. 4a**,**b**,**e** and **Table 1**). The pre-B cells in *Atp11c*$^{amb/0}$ *Vav-Bcl2* mice nevertheless did not have higher expression of CD24 (**Fig. 4b**) or CD25 (**Supplementary Fig. 8a**). Immature B cells were also partly restored in *Atp11c*$^{amb/0}$ *Vav-Bcl2* mice, although they still represented only 17% of the numbers in *Atp11c*$^{+/0}$ *Vav-Bcl2* control mice (**Fig. 4e** and **Table 1**). Likewise, spleen B cells remained at 6% of the number in *Atp11c*$^{+/0}$ *Vav-Bcl2* control mice and 31% of that in

Table 1 B cells in the spleen and B cell subpopulations in bone marrow

ATP11C	Transgene	Pre-pro-B cells	Pro-B cells	Pre-B cells	Immature B cells	Mature B cells	Mice (*n*; BM)	Splenic B cells	Mice (*n*; spleen)
WT	None	3.99 ± 0.25	4.10 ± 0.42	28.66 ± 2.04	12.50 ± 1.20	14.29 ± 0.89	14	20.06 ± 1.87	11
Amb	None	5.55 ± 0.36	2.22 ± 0.42	1.74 ± 0.34	0.24 ± 0.04	1.75 ± 0.25	13	1.73 ± 0.20	10
WT	*Vav-Bcl2*	5.53 ± 0.48	6.48 ± 0.65	21.48 ± 5.72	17.60 ± 1.65	69.63 ± 13.55	4	101.10 ± 11.84	4
Amb	*Vav-Bcl2*	6.22 ± 0.49	4.78 ± 0.96	6.22 ± 1.37	3.12 ± 0.26	9.98 ± 1.06	6	6.18 ± 1.37	6
WT	*H2Ea-Il7*	2.36 ± 0.56	19.26 ± 2.28	262.00 ± 36.5	36.36 ± 3.86	1.66 ± 0.31	5	153.30 ± 18.25	3
Amb	*H2Ea-Il7*	5.33 ± 0.21	2.33 ± 0.40	1.68 ± 0.43	0.25 ± 0.03	6.30 ± 1.45	4	7.78 ± 1.94	2
WT	MD4	2.53 ± 0.29	0.50 ± 0.06	0.73 ± 0.13	15.97 ± 0.89	10.07 ± 0.84	3	10.82 ± 1.64	3
Amb	MD4	3.28 ± 0.32	0.70 ± 0.03	0.66 ± 0.03	1.98 ± 0.39	4.90 ± 1.04	5	3.00 ± 0.23	5

Pre-pro-B cells (CD24$^-$CD43$^+$ in the IgD$^-$IgM$^-$ gate), pro-B cells (CD24^{int}CD43$^+$ in the IgD$^-$IgM$^-$ gate), pre-B cells (CD24^{hi}CD43$^-$ in the IgD$^-$IgM$^-$ gate), immature B cells (IgD$^-$IgM$^+$ in the B220$^+$ gate) and mature B cells (IgD$^+$ IgM$^+$ in B220$^+$ gate) in the bone marrow (BM; ×10^5), and B cells (B220$^+$ in live lymphocytes gate) in the spleen (×10^6). Data are pooled from two to three experiments (mean ± s.e.m.).

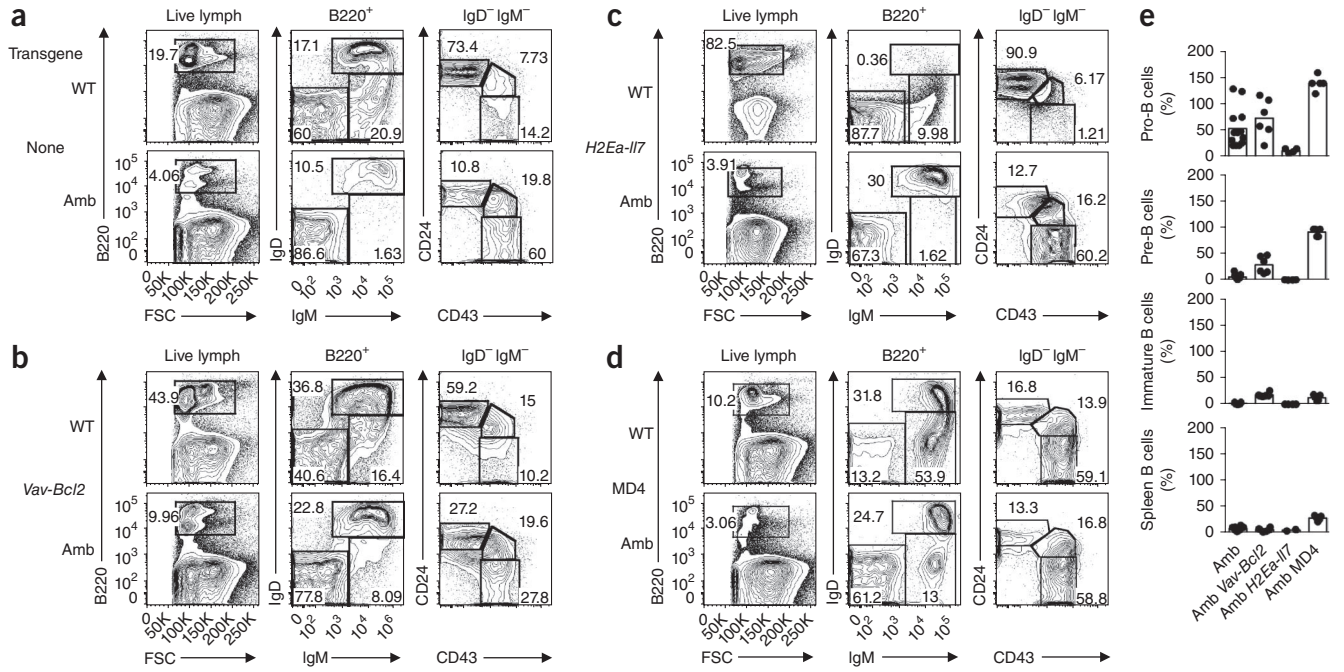

Figure 4 Effects of transgenes encoding Bcl-2, IL-7 or the BCR on the development of ATP11C-mutant B cells. (**a**–**d**) Flow cytometry showing the frequency of B cell subpopulations in the bone marrow of mice with wild-type or mutant ATP11C and no transgene (**a**), the *Vav-Bcl2* transgene (**b**), the *H2Ea-Il7* transgene (**c**) or the MD4 transgene (**d**). Numbers adjacent to outlined areas indicate percent cells in each. (**e**) Pro-B cells, pre-B cells and immature B cells in the bone marrow and B cells in the spleen of mice as in **a**–**d**, presented relative to those in *Atp11c*$^{+/0}$ wild-type control mice with the same transgene or of the same line. Each symbol represents an individual mouse. Data are representative of two to five experiments (**a**–**d**) or are pooled from two to three experiments (**e**) with one to five mice of each genotype in each (mean and individual values in **e**).

wild-type mice, and they continued to have high expression of IgM. Suppression of apoptosis by enforced Bcl-2 expression was therefore unable to correct the B cell developmental abnormalities caused by ATP11C deficiency.

H2Ea-Il7 mice with a normal *Atp11c* gene had fivefold more bone marrow pro-B cells and tenfold more pre-B cells than did wild-type mice (**Fig. 4c**,**e** and **Table 1**), consistent with published analyses[27]. In contrast, there was no effect of the greater abundance of IL-7 on the number of pro-B cells, pre-B cells or immature B cells in *Atp11c*$^{amb/0}$ *H2Ea-Il7* mice relative to that in *Atp11c*$^{amb/0}$ mice without *H2Ea-Il7* (**Table 1**). More IL-7 was therefore unable to restore the development of ATP11C-deficient B cells and instead the mutation abolished the effects of transgenic expression of IL-7 on pro-B cells and pre-B cells in the bone marrow.

In MD4 mice, the rearranged immunoglobulin heavy- and light-chain transgenes are normally activated during the pro-B cell stage, bypassing and suppressing recombination of the endogenous immunoglobulin genes mediated by the RAG recombinase. This resulted in a lower number of pro-B cells and pre-B cells, to 12% and 2% of normal numbers, respectively, and replacement of those cells with immature IgM$^+$IgD$^-$B cells present in normal numbers in the bone marrow (**Table 1**). Whereas the *Atp11c*^{amb} mutation resulted in fewer pro-B cells in non-transgenic mice, it resulted in more pro-B cells in MD4 mice, at 150% of the number in control MD4 mice with normal ATP11C (**Fig. 4e** and **Table 1**). As discussed below, the greater abundance of pro-B cells probably reflected a developmental delay in activation of the rearranged immunoglobulin transgenes in the *Atp11c*$^{amb/0}$ pro-B cell population. The number of immature B cells in the bone marrow of *Atp11c*$^{amb/0}$ MD4 mice was nevertheless only partly restored to 11% of the number in *Atp11c*$^{+/0}$ MD4 mice, whereas spleen and circulating B cells were partly restored to 37% of those in MD4 mice with normal ATP11C. There was a similar magnitude of restoration in SW_{HEL} mice with a rearranged immunoglobulin heavy-chain gene complex (*Igh*) targeted in its normal location, but only when that was combined with a rearranged transgenic light chain (**Supplementary Fig. 8b**). Bypassing the pre-BCR signaling step thus alleviated but did not eliminate the need for ATP11C.

To further characterize the developmental block in bone marrow B cells, we stained cells for cytoplasmic-μ (cμ) heavy chains in mIgM$^-$B220^{lo} cells, comparing wild-type or *Atp11c*$^{amb/0}$ mice with mice homozygous for null mutations eliminating the RAG-1 recombinase or the CD79α (immunoglobulin-α) subunit of the pre-BCR and BCR. In wild-type mice, 65% of mIgM$^-$B220^{lo} cells were cμ$^+$, and these were CD24^{hi} because of pre-BCR signaling (**Fig. 5a**,**b**). No mIgM$^-$B220^{lo} cells were cμ$^+$ in mice deficient in recombination-activating gene 1 (*Rag1*$^{-/-}$), consistent with their inability to recombine the heavy-chain genes. We found that 15% of mIgM$^-$B220^{lo} cells were cμ$^+$ in *Cd79a*$^{-/-}$ marrow, and their low frequency and lower CD24 expression was consistent with the inability of the pre-BCR to assemble and signal. Relative to this baseline frequency of cells with functionally rearranged but unselected IgM heavy-chain genes, the frequency of cμ$^+$ cells was even lower in *Atp11c*$^{amb/0}$ mice, representing only 5% of mIgM$^-$B220^{lo} cells (**Fig. 5a**,**b**).

As IL-7 is important for the proliferation of pro-B cells and pre-B cells, we investigated whether their proliferation was diminished by ATP11C deficiency *in vivo* or *in vitro*. Flow cytometry analysis of bone marrow pre-pro-B cells, pro-B cells and pre-B cells stained for DNA content showed a greater frequency of mutant pro-B cells and pre-B cells with >2n DNA (**Fig. 5c**,**d**), which indicated that a greater proportion of mutant pro-B cells and pre-B cells were in the S phase

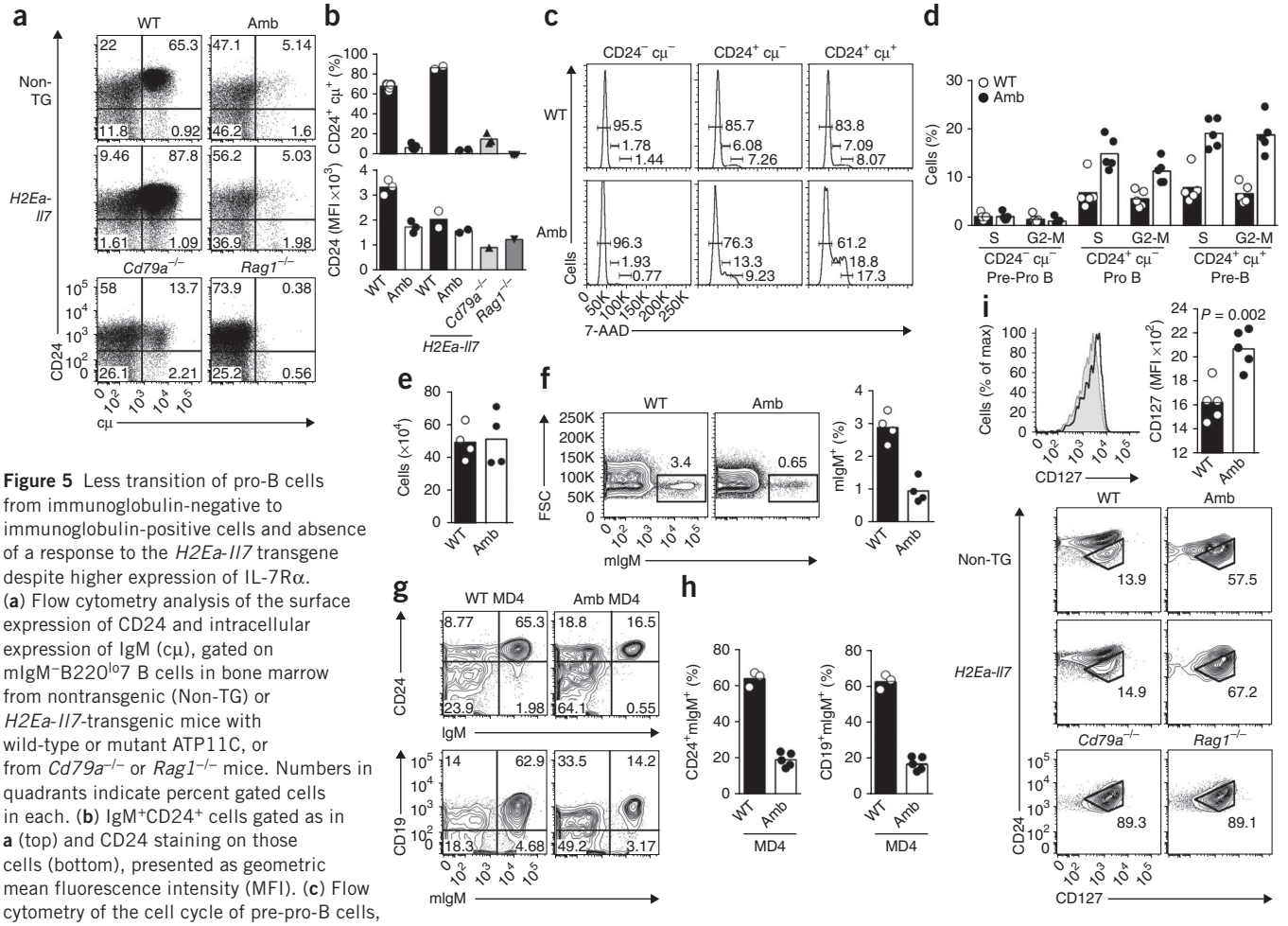

Figure 5 Less transition of pro-B cells from immunoglobulin-negative to immunoglobulin-positive cells and absence of a response to the *H2Ea-Il7* transgene despite higher expression of IL-7Rα. (**a**) Flow cytometry analysis of the surface expression of CD24 and intracellular expression of IgM (cμ), gated on mIgM$^-$B220^{lo}7 B cells in bone marrow from nontransgenic (Non-TG) or *H2Ea-Il7*-transgenic mice with wild-type or mutant ATP11C, or from *Cd79a*$^{-/-}$ or *Rag1*$^{-/-}$ mice. Numbers in quadrants indicate percent gated cells in each. (**b**) IgM$^+$CD24$^+$ cells gated as in **a** (top) and CD24 staining on those cells (bottom), presented as geometric mean fluorescence intensity (MFI). (**c**) Flow cytometry of the cell cycle of pre-pro-B cells, pro-B cells and pre-B cells. Numbers adjacent to bracketed lines indicate percent cycling cells in G0-G1 (left), S (middle) or G2-M (right). (**d**) Frequency of pre-pro-B cells, pro-B cells and pre-B cells in S or G2-M phase. (**e**) Absolute number of cells after 7 d of culture of sorted pro-B cells in the presence of IL-7 (25 ng/ml). (**f**) Flow cytometry analysis of mIgM on live B220$^+$ cells after culture as in **e**. Numbers above outlined areas indicate percent mIgM$^+$ cells among all live B220$^+$ cells (**g**). Flow cytometry of bone marrow from MD4 mice, assessing surface expression of IgM and CD24 (top) or CD19 (bottom) by B220^{lo}IgD$^-$ cells. Numbers in quadrants indicate percent cells in each. (**h**) Frequency of CD24$^+$mIgM$^+$ cells (left) or CD19$^+$mIgM$^+$ cells (right) among the cells in **g**. (**i**) Expression of CD127 (IL-7Rα) on CD24^{int}CD43$^+$CD19$^+$IgM$^-$B220^{lo} pro-B cells (top left) from *Atp11c*$^{amb/0}$ mice (black line) and wild-type mice (shaded histogram) and CD127 fluorescence on pro-B cells (top right). *P* value, Student's *t*-test. Below, flow cytometry of CD24 versus CD127 on CD19$^+$IgM$^-$B220^{lo}7-AAD$^-$ cells in bone marrow from nontransgenic or *H2Ea-Il7*-transgenic mice with wild-type or mutant ATP11C, or from *Cd79a*$^{-/-}$ and *Rag1*$^{-/-}$ mice. Numbers adjacent to outlined areas indicate percent cells of the CD24^{int} pro-B cell subset. Each symbol (**b**,**d**–**f**,**h**,**i**) represents an individual mouse. Data are representative of two to five (**a**) or two (**c**) experiments, three separate experiments with one to four mice per group in each (**b**,**e**,**f**,**i**) or two separate experiments with two to five mice per group in each (**d**), or are combined from three separate experiments with one to three mice per group in each (**g**,**h**).

or the G2 and M phases of the cell cycle. When we sorted pro-B cells by flow cytometry and cultured them with high concentrations of IL-7 (25 ng/ml), we found that mutant and wild-type pro-B cells increased in number identically over 7 d, whether measured in separate cultures or by comparison of their ratios in competitive cocultures (**Fig. 5e** and data not shown). However, when we analyzed the differentiation of these cells by measuring the fraction that had become small pre-B cells and mIgM$^+$ immature B cells, we found that a much smaller fraction of the mutant pro-B cells had differentiated (**Fig. 5f**). These results indicate that mutation of *Atp11c* does not interfere with the proliferation of pro-B cells but disrupts their differentiation into pre-B cells and immature B cells.

The cμ$^+$ cells in *Atp11c*$^{amb/0}$ marrow had more CD24, but was still only half that on normal cμ$^+$ cells. When the need for immunoglobulin gene rearrangement and pre-BCR signaling was bypassed in MD4 mice, ATP11C deficiency still resulted in a much lower frequency of B220^{lo} B cells expressing the immunoglobulin genes, and instead there was an expanded population of pro-B cells that had not yet activated immunoglobulin transgene expression (**Fig. 5g**,**h** and **Table 1**). Collectively, these results indicate that the onset of heavy-chain expression and the response to pre-BCR assembly are both diminished in the absence of normal ATP11C.

Normally, cμ$^+$ cells show a heightened proliferative response to IL-7 as a result of synergy between IL-7R and pre-BCR signaling[10,11], so populations of cμ$^+$ cells among mIgM$^-$B220^{lo} cells were 'preferentially' expanded in *H2Ea-Il7* mice (**Fig. 5a**,**b**). Like the data about pro-B and pre-B cell numbers reported above (**Table 1**), this effect of *H2Ea-Il7* was also completely abolished by the *Atp11c*^{amb} mutation, so that the low frequency of cμ$^+$ cells in *Atp11c*$^{amb/0}$ marrow remained unchanged by *H2Ea-Il7*. Expression of IL-7Rα (CD127) on CD19$^+$CD24^{int}mIgM$^-$B220^{lo} pro-B cells was nevertheless significantly higher in *Atp11c*$^{amb/0}$ mice and *Atp11c*$^{amb/0}$ *H2Ea-Il7* mice than in

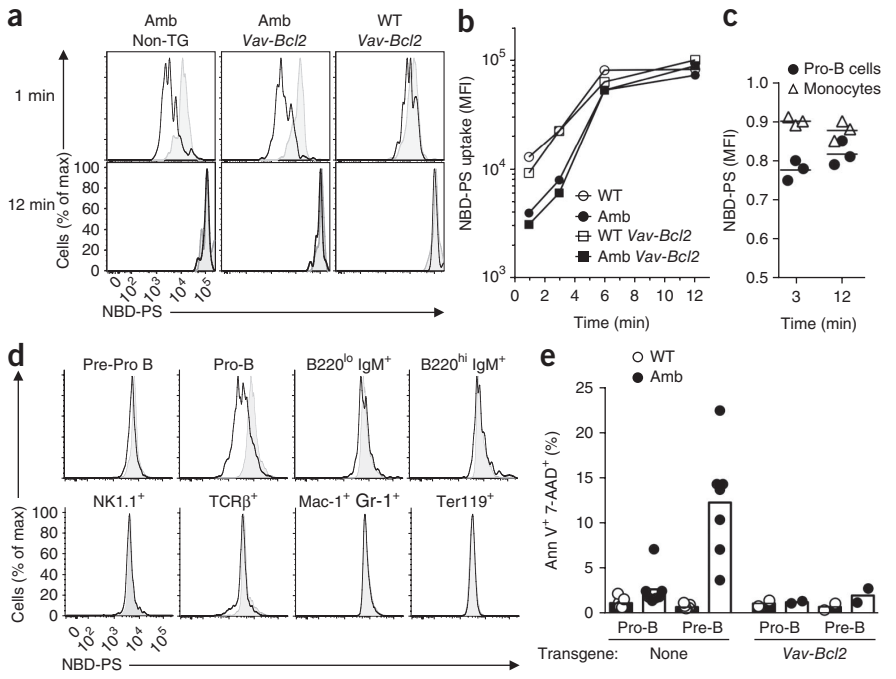

Figure 6 The *Atp11c*^{amb} mutation results in less translocation of PS into pro-B cells. (**a**) NBD-PS fluorescence profiles of pro-B cells from mice with wild-type or mutant ATP11C lacking (Non-TG) or carrying the *Vav-Bcl2* transgene (black lines) and of the corresponding CD45.1$^+$ wild-type pro-B cells (shaded histograms), after 1 or 12 min of incubation. (**b**) NBD-PS in pro-B cells of mice (genotypes as in **a**) after 0–12 min of incubation, presented as geometric mean fluorescence intensity. (**c**) NBD-PS in bone marrow pro-B cells or monocytes from *Atp11c*$^{amb/0}$ mice, presented as fluorescence intensity relative to that of CD45.1$^+$ wild-type pro-B cells or monocytes. Each symbol represents an individual mouse; small horizontal lines indicate the mean. (**d**) NBD-PS fluorescence profiles in pre-pro-B cells, pro-B cells, B220^{lo}IgM$^+$ cells, B220^{hi}IgM$^+$ cells, NK1.1$^+$ cells, TCRβ$^+$ cells, Mac-1$^+$Gr-1$^+$ cells and Ter119$^+$ cells from ATP11C-mutant bone marrow (black lines), assessed after 1 min incubation and presented relative to that of the corresponding CD45.1$^+$ wild-type bone marrow cells (shaded histograms). (**e**) Apoptotic pro-B cells or pre-B cells from mice with wild-type or mutant ATP11C with or without the *Vav-Bcl2* transgene, assessed as positive staining for annexin V (AnnV) and 7-AAD. Each symbol represents an individual mouse. Data are representative of two to three experiments (**a**–**d**) or are from two experiments (nontransgenic) or one experiment (*Vav-Bcl2*) with two to five mice per group in each (**e**).

wild-type control mice (**Fig. 5i**), which indicated that the absence of an *in vivo* response to *H2Ea-Il7* was not explained by failure to express the receptor.

Lower PS flippase activity

The evidence reported above indicating that pro-B cells did not differentiate or respond to IL-7 normally focused our analysis on testing of this cell subset for aminophospholipid flippase activity. We mixed bone marrow from CD45.2$^+$ *Atp11c*$^{amb/0}$ mice and CD45.1$^+$ *Atp11c*$^{+/0}$ control mice and incubated the mixture for various amounts of time with the fluorescent PS analog NBD-PS. We then extracted any dye remaining in the exoplasmic leaflet with lipid-free albumin and washed it away. We distinguished the mutant and control pro-B cell subsets by antibody staining and analyzed them by flow cytometry. NBD-PS fluorescence in mutant and wild-type pro-B cells increased rapidly and approached saturation by 12 min at 37 °C but was homogeneously less in mutant pro-B cells analyzed at 1 or 3 min (**Fig. 6a**,**b**). The lower PS flippase activity in *Atp11c*$^{amb/0}$ pro-B cells was not corrected by enforced expression of Bcl-2 and was selective for pro-B cells, as it was not as great in mutant monocytes present in the same samples (**Fig. 6a**–**c**). Comparison of a broad range of bone marrow cell types showed that the flippase defect was specific not only for the B lineage but also for the pro-B cell stage (**Fig. 6d**), which indicated close correlation between flippase activity and cell development. The pre-pro-B cells and the immature and mature B cells in the bone marrow, as well as follicular and marginal zone B cells in the spleen of mutant mice, all showed normal flippase activity (**Fig. 6d** and **Supplementary Fig. 9a**). Notably, the only other blood cell types with lower flippase activity in ATP11C-mutant mice were CD4$^-$CD8$^-$ double-negative thymocytes and CD4$^+$CD8$^+$ double-positive thymocytes (**Supplementary Fig. 9b**). As in pro-B cells, the flippase deficit was stage specific in the T cell lineage, as flippase activity was normal in mature T cells in bone marrow and spleen and in CD4$^+$ or CD8$^+$ single-positive thymocytes (**Fig. 6d** and **Supplementary Fig. 9a**,**b**). However, the lower flippase activity did not cause an obvious defect in the differentiation of double-positive cells into single-positive cells (data not shown). Together these data show that ATP11C is critical for phospholipid flipping in a developmental stage–dependent way and that the B cell lineage is uniquely sensitive to lower flippase activity despite its nearly ubiquitous expression of ATP11C (**Supplementary Fig. 10**).

To determine if the *Atp11c*^{amb} mutation led to a steady-state increase in the concentration of PS in the exoplasmic plasma membrane leaflet of pro-B cells, we stained bone marrow cells with the PS-binding protein annexin V and the membrane-impermeable DNA dye 7-aminoactinomycin D (7-AAD). There was no greater annexin V fluorescence on viable 7-AAD$^-$ pro-B cells or pre-B cells from *Atp11c*$^{amb/0}$ mice, but the frequency of apoptotic cells stained with both annexin V and 7-AAD was greater among pre-B cells from *Atp11c*$^{amb/0}$ mice (**Fig. 6e**). This greater abundance of apoptotic pre-B cells was suppressed by enforced expression of Bcl-2 (**Fig. 6e**), which indicated that it was an indirect effect of ATP11C deficiency. Thus, the rate of translocation of PS into the inner leaflet was lower in ATP11C-deficient pro-B cells but remained sufficient to prevent measurable accumulation of PS in the exoplasmic leaflet unless the cells entered apoptosis.

DISCUSSION

Our study has elucidated a previously unknown connection among specialized membrane lipid partitioning, B cell differentiation and antigen-specific antibody production. A previously unstudied member of the large family of P4-type ATPases, ATP11C, was required for efficient PS flippase activity in developing B lymphocytes and was essential for normal B cell differentiation from the pro-B cell stage onward. As a result of *Atp11c* mutation, fewer pro-B cells expressed rearranged *Igh* genes, pro-B cells and pre-B cells seemed unresponsive to supraphysiological concentrations of IL-7 *in vivo* and differentiated

poorly during IL-7 driven proliferation *in vitro*, there was poor induction of CD24 and CD25 on pre-BCR expressing cells, and a greater percentage of pre-B cells were apoptotic. Little is understood about the relationship between the composition of the inner leaflet of the plasma membrane and cytokine receptor or antigen receptor signaling, and the discovery that ATP11C is critical for B cell differentiation opens up a new avenue with which to bridge this gap.

As for the biochemical function of ATP11C, the simplest interpretation of the data is that it is an essential aminophospholipid flippase in the plasma membrane of pro-B cells, because PS flippase activity was lower in cells with the *Atp11c*^{amb} mutation even when apoptosis was blocked by Bcl-2, and other members of this protein family have been shown to be PS flippases in biochemical reconstitution and yeast genetic studies[14,21–23]. However, analyses of yeasts with mutant P4 ATPases have underscored the potential for effects on protein or organelle trafficking and cell metabolism that could indirectly affect PS flippase activity[14,30–32]. Further research is needed to confirm the PS flippase activity of ATP11C by biochemical reconstitution studies and to assess its activity for phosphatidylethanolamine and phosphatidylinositol that are also concentrated in the cytoplasmic leaflet. The observation that PS flippase activity was lower but by no means abolished in ATP11C-mutant pro-B cells indicates that other aminophospholipid flippases also act in B cells, consistent with the relatively ubiquitous mRNA expression of many other P4 ATPase family members.

How might the loss of one flippase have such a specific and large effect on the differentiation of pro-B cells? The data indicate a direct or indirect defect in the response to IL-7R and the pre-BCR. In contrast to B cells in *Il7*$^{-/-}$ or *Il7ra*$^{-/-}$ mice, which have complete absence of IL-7R signaling[33] and thus B cells fail to develop to the pro-B cell stage, B cells in ATP11C-mutant mice developed into pro-B cells, proliferated normally and showed an arrest similar to that in *Il7ra*$^{-/-}$ *Vav-Bcl2* mice[34]. Both the *in vivo* and *in vitro* defects could all reflect some critical qualitative element of IL-7 signaling or could be secondary, as there is known to be a complex feed-forward loop among IL-7 signaling, B cell transcription factors and pre-BCR signaling[1–4]. The greater abundance of IL-7R on the surface of mutant pro-B cells may reflect less signaling through IL-7R, as binding of IL-7 to IL-7R normally leads to rapid endocytosis of the receptor via the clathrin-coated pits necessary for efficient signal transduction[35], and IL-7R signaling normally diminishes the transcription of IL-7R mRNA[36,37]. The biophysics of antigen receptor or IL-7R signaling is not well understood, but several independent observations provide possible connections with PS concentrations in the cytoplasmic membrane leaflet and in lipid rafts. PS is most concentrated on the inner leaflet of the plasma membrane at endocytic cups and early endosomes[13] and in lipid rafts associated with the T cell antigen receptor[38], where it serves as a binding site and regulatory factor for proteins with cationic or C2-domains, such as proteins of the Src, Ras, Rho and PKC families[13], and for binding the cationic stretch that precedes immunoreceptor tyrosine-based activation motifs in subunits of the CD3 invariant signaling protein[39,40]. The efficiency of IL-7R signaling has also been linked to its association with lipid rafts[41,42]. PS has also been found to be externalized and capped together with the BCR during BCR or pre-BCR signaling[43]. Thus, future studies should test the consequences of *Atp11c* mutation on the accumulation of PS and signal-transducing proteins at subcellular patches where IL-7, pre-BCR or BCR signaling has been initiated.

Why were B cells profoundly compromised by the *Atp11c*^{amb} mutation, whereas T cells and most other tissues seemed normal? Microarray profiling of ATP11C mRNA has shown that it has equal expression in B lymphocytes and T lymphocytes (data not shown) and most other tissues, with its highest expression in liver[44]. PS flippase activity was nevertheless also lower in double-negative and double-positive pro-T cells and pre-T cells, yet the mutation selectively compromised differentiation of pro-B cells. The simplest explanation may be redundancy between ATP11C and other P4 ATPases in other B cell stages and lineages. Alternatively, post-translational regulatory changes in phospholipid flippase, floppase and 'scramblase' activity and unique membrane events required in bone marrow pro-B and pre-B cells may explain the stage- and lineage-specific dependence on ATP11C. The profound requirement for ATP11C in pro-B lymphocytes and pre-B lymphocytes provides a unique experimental avenue for understanding the connections between membrane phospholipid distribution and cell biological functions that are probably important for many other cell types, and may provide a new drug target for the treatment of B cell malignancy. The X-chromosomal location of human *ATP11C* makes it a candidate for inherited B cell deficiency and hepatocellular carcinoma in men.

METHODS

Methods and any associated references are available in the online version of the paper at http://www.nature.com/natureimmunology/.

Note: Supplementary information is available on the Nature Immunology website.

ACKNOWLEDGMENTS

We thank the staff of the Australian National University Bioscience Research Services for animal husbandry; the Australian Phenomics Facility genotyping and mapping team for genetic analysis; D. Howard for help with the bone marrow chimeras; A. Bröer for help with the flippase assay; staff of the John Curtin School of Medical Research microscopy and flow cytometry resource facility for help with flow cytometry; the Biomolecular Resource Facility of the Australian Cancer Research Foundation and the Australian Genome Research Facility for DNA sequencing; and K. Peng (Biomolecular Resource Facility of the Australian Cancer Research Foundation), John Curtin School of Medical Research and the Australian Genome Research Facility Next Generation Sequencing and Bioinformatics teams, Brisbane, for preparing and running samples in parallel for next-generation sequencing. Supported by the National Institutes of Health (C.C.G.), Wellcome Trust (C.C.G.), the Australian Research Council (C.C.G.), the National Health and Medical Research Council (C.C.G.), the Ramaciotti Foundation (C.C.G. and A.E.), the Ministry of National Education, Republic of Turkey (M.Y.) and Deutsche Forschungsgemeinschaft (EN 790/1-1 to A.E.).

AUTHOR CONTRIBUTIONS

M.Y. did and analyzed most of the experiments; C.E.T., S.F., D.L. E.M.K., J.K. and A.E. contributed to experiments; C.M.R. and A.E. identified the ATP11C-mutant strains; B.W., D.T.A., Y.Z. and A.E. mapped and identified the mutation in the ambrosius strain; N.C.T. and G.C.F. analyzed liver histology and clinical chemistry; S.B. helped with the flippase assay; C.C.G. and A.E. conceived of the research and directed the study; and M.Y., C.C.G. and A.E. prepared the figures and wrote the paper in consultation with all authors.

COMPETING FINANCIAL INTERESTS

The authors declare no competing financial interests.

Published online at http://www.nature.com/natureimmunology/.
Reprints and permissions information is available online at http://npg.nature.com/reprintsandpermissions/.

1. Malin, S., Mcmanus, S. & Busslinger, M. STAT5 in B cell development and leukemia. *Curr. Opin. Immunol.* **22**, 168–176 (2010).
2. Ye, M. & Graf, T. Early decisions in lymphoid development. *Curr. Opin. Immunol.* **19**, 123–128 (2007).
3. Mandel, E.M. & Grosschedl, R. Transcription control of early B cell differentiation. *Curr. Opin. Immunol.* **22**, 161–167 (2010).
4. Nutt, S.L. & Kee, B.L. The transcriptional regulation of B cell lineage commitment. *Immunity* **26**, 715–725 (2007).
5. Welner, R.S., Pelayo, R. & Kincade, P.W. Evolving views on the genealogy of B cells. *Nat. Rev. Immunol.* **8**, 95–106 (2008).
6. Hardy, R.R., Kincade, P.W. & Dorshkind, K. The protean nature of cells in the B lymphocyte lineage. *Immunity* **26**, 703–714 (2007).

7. Inlay, M.A. *et al.* Ly6d marks the earliest stage of B-cell specification and identifies the branchpoint between B-cell and T-cell development. *Genes Dev.* **23**, 2376–2381 (2009).
8. Wei, C., Zeff, R. & Goldschneider, I. Murine pro-B cells require IL-7 and its receptor complex to up-regulate IL-7Rα, terminal deoxynucleotidyltransferase, and cμ expression. *J. Immunol.* **164**, 1961–1970 (2000).
9. Melchers, F. The pre-B-cell receptor: selector of fitting immunoglobulin heavy chains for the B-cell repertoire. *Nat. Rev. Immunol.* **5**, 578–584 (2005).
10. Fleming, H.E. & Paige, C.J. Pre-B cell receptor signaling mediates selective response to IL-7 at the pro-B to pre-B cell transition via an ERK/MAP kinase-dependent pathway. *Immunity* **15**, 521–531 (2001).
11. Marshall, A.J., Fleming, H.E., Wu, G.E. & Paige, C.J. Modulation of the IL-7 dose-response threshold during pro-B cell differentiation is dependent on pre-B cell receptor expression. *J. Immunol.* **161**, 6038–6045 (1998).
12. Lingwood, D. & Simons, K. Lipid rafts as a membrane-organizing principle. *Science* **327**, 46–50 (2010).
13. Leventis, P.A. & Grinstein, S. The distribution and function of phosphatidylserine in cellular membranes. *Annu Rev Biophys* **39**, 407–427 (2010).
14. Muthusamy, B.-P., Natarajan, P., Zhou, X. & Graham, T.R. Linking phospholipid flippases to vesicle-mediated protein transport. *Biochim. Biophys. Acta* **1791**, 612–619 (2009).
15. Yeung, T. *et al.* Membrane phosphatidylserine regulates surface charge and protein localization. *Science* **319**, 210–213 (2008).
16. Park, D. *et al.* BAI1 is an engulfment receptor for apoptotic cells upstream of the ELMO/Dock180/Rac module. *Nature* **450**, 430–434 (2007).
17. Miyanishi, M. *et al.* Identification of Tim4 as a phosphatidylserine receptor. *Nature* **450**, 435–439 (2007).
18. Dillon, S.R., Constantinescu, A. & Schlissel, M.S. Annexin V binds to positively selected B cells. *J. Immunol.* **166**, 58–71 (2001).
19. Holder, M.J., Barnes, N.M., Gregory, C.D. & Gordon, J. Lymphoma cells protected from apoptosis by dysregulated bcl-2 continue to bind annexin V in response to B-cell receptor engagement: a cautionary tale. *Leuk. Res.* **30**, 77–80 (2006).
20. Pomorski, T. & Menon, A.K. Lipid flippases and their biological functions. *Cell. Mol. Life Sci.* **63**, 2908–2921 (2006).
21. Tang, X., Halleck, M.S., Schlegel, R.A. & Williamson, P. A subfamily of P-type ATPases with aminophospholipid transporting activity. *Science* **272**, 1495–1497 (1996).
22. van der Velden, L.M., van de Graaf, S.F.J. & Klomp, L.W.J. Biochemical and cellular functions of P4 ATPases. *Biochem. J.* **431**, 1–11 (2010).
23. Paulusma, C.C. & Elferink, R.P.J.O. P4 ATPases–the physiological relevance of lipid flipping transporters. *FEBS Lett.* **584**, 2708–2716 (2010).
24. Bull, L.N. *et al.* A gene encoding a P-type ATPase mutated in two forms of hereditary cholestasis. *Nat. Genet.* **18**, 219–224 (1998).
25. Siggs, O.M. *et al.* The P4-type ATPase ATP11C is essential for B lymphopoiesis in adult bone marrow. *Nat. Immunol.* advance online publication, doi:10.1038/ni.2012 (20 March 2011).
26. Ogilvy, S. *et al.* Constitutive Bcl-2 expression throughout the hematopoietic compartment affects multiple lineages and enhances progenitor cell survival. *Proc. Natl. Acad. Sci. USA* **96**, 14943–14948 (1999).
27. Mertsching, E., Grawunder, U., Meyer, V., Rolink, T. & Ceredig, R. Phenotypic and functional analysis of B lymphopoiesis in interleukin-7-transgenic mice: expansion of pro/pre-B cell number and persistence of B lymphocyte development in lymph nodes and spleen. *Eur. J. Immunol.* **26**, 28–33 (1996).
28. Goodnow, C.C. *et al.* Altered immunoglobulin expression and functional silencing of self-reactive B lymphocytes in transgenic mice. *Nature* **334**, 676–682 (1988).
29. Phan, T.G. *et al.* B cell receptor-independent stimuli trigger immunoglobulin (Ig) class switch recombination and production of IgG autoantibodies by anergic self-reactive B cells. *J. Exp. Med.* **197**, 845–860 (2003).
30. Gall, W.E. *et al.* Drs2p-dependent formation of exocytic clathrin-coated vesicles in vivo. *Curr. Biol.* **12**, 1623–1627 (2002).
31. Hua, Z., Fatheddin, P. & Graham, T.R. An essential subfamily of Drs2p-related P-type ATPases is required for protein trafficking between Golgi complex and endosomal/vacuolar system. *Mol. Biol. Cell* **13**, 3162–3177 (2002).
32. Alder-Baerens, N., Lisman, Q., Luong, L., Pomorski, T. & Holthuis, J.C.M. Loss of P4 ATPases Drs2p and Dnf3p disrupts aminophospholipid transport and asymmetry in yeast post-Golgi secretory vesicles. *Mol. Biol. Cell* **17**, 1632–1642 (2006).
33. Kikuchi, K., Lai, A.Y., Hsu, C.-L. & Kondo, M. IL-7 receptor signaling is necessary for stage transition in adult B cell development through up-regulation of EBF. *J. Exp. Med.* **201**, 1197–1203 (2005).
34. Malin, S. *et al.* Role of STAT5 in controlling cell survival and immunoglobulin gene recombination during pro-B cell development. *Nat. Immunol.* **11**, 171–179 (2010).
35. Henriques, C.M., Rino, J., Nibbs, R.J., Graham, G.J. & Barata, J.T. IL-7 induces rapid clathrin-mediated internalization and JAK3-dependent degradation of IL-7Rα in T cells. *Blood* **115**, 3269–3277 (2010).
36. Alves, N.L., van Leeuwen, E.M.M., Derks, I.A.M. & van Lier, R.A.W. Differential regulation of human IL-7 receptor α expression by IL-7 and TCR signaling. *J. Immunol.* **180**, 5201–5210 (2008).
37. Park, J.-H. *et al.* Suppression of IL7Ralpha transcription by IL-7 and other prosurvival cytokines: a novel mechanism for maximizing IL-7-dependent T cell survival. *Immunity* **21**, 289–302 (2004).
38. Zech, T. *et al.* Accumulation of raft lipids in T-cell plasma membrane domains engaged in TCR signalling. *EMBO J.* **28**, 466–476 (2009).
39. Xu, C. *et al.* Regulation of T cell receptor activation by dynamic membrane binding of the CD3epsilon cytoplasmic tyrosine-based motif. *Cell* **135**, 702–713 (2008).
40. Aivazian, D. & Stern, L.J. Phosphorylation of T cell receptor zeta is regulated by a lipid dependent folding transition. *Nat. Struct. Biol.* **7**, 1023–1026 (2000).
41. Cho, J.-H., Kim, H.-O., Surh, C.D. & Sprent, J. T Cell receptor-dependent regulation of lipid rafts controls naive $CD8^+$ T cell homeostasis. *Immunity* **32**, 214–226 (2010).
42. Rose, T. *et al.* Interleukin-7 compartmentalizes its receptor signaling complex to initiate CD4 T lymphocyte response. *J. Biol. Chem.* **285**, 14898–14908 (2010).
43. Dillon, S.R., Mancini, M., Rosen, A. & Schlissel, M.S. Annexin V binds to viable B cells and colocalizes with a marker of lipid rafts upon B cell receptor activation. *J. Immunol.* **164**, 1322–1332 (2000).
44. Wu, C. *et al.* BioGPS: an extensible and customizable portal for querying and organizing gene annotation resources. *Genome Biol.* **10**, R130 (2009).

ONLINE METHODS

Mice and procedures. The ambrosius mouse strain was generated by *N*-ethyl-*N*-nitrosourea mutagenesis on a pure C57BL/6 background at the Australian Phenomics Facility of the Australian National University as described[45]. The strain was maintained by breeding of affected males with littermates or with wild-type C57BL/6 females and, for mapping purposes, was crossed to the CBA/H strain. *Vav-Bcl2*-transgenic mice[46], *H2Ea-Il7*-transgenic mice[27], the MD4 line[28] and *Rag1*$^{-/-}$ mice[47] have been described. The *Cd79a*$^{-/-}$ mouse strain has a point mutation in *Cd79a* that leads to a premature stop codon in exon 2 (L.E.T. and A.E., unpublished data). Except where noted otherwise, all mice used for this study were between 8 and 12 weeks of age. All experimental mice were maintained on a C57BL/6 background and were housed in specific pathogen–free conditions at the Australian Phenomics Facility and all animal procedures were approved by the Australian National University Animal Ethics and Experimentation Committee. Strains are available from the Australian Phenome Bank.

Primary immunization with 50 µg ABA-CGG (Biosearch) or 1×10^8 heat- and formalin-inactivated *B. pertussis* bacteria (Lee Laboratories) and booster immunization with ABA-CGG or 25 µg nitrophenyl-Ficoll (Biosearch) and detection of antibodies by enzyme-linked immunosorbent assay were done as described[47]. An ADVIA 2120 Haematology System (Siemens Healthcare Diagnostics) was used for differential absolute blood counts.

Serum concentrations of alanine aminotransferase, aspartate aminotransferase and bilirubin were assayed by automated procedures in the Department of Pathology of The Canberra Hospital.

Tumor collection and histology. Liver tumors and surrounding liver tissue were removed and fixed in 10% (vol/vol) neutral buffered formalin. Liver sections 4 µm in thickness were cut from paraffin-embedded blocks and were stained with hematoxylin and eosin for histological examination.

Sequencing and mutation identification. A SureSelect custom solution array (Agilent) was designed with the online tool eArray to include annotated exons (plus splice-donor and splice-acceptor sites) in the chromosome X-linkage interval from position 54012901 to position 60897610 of RefSeq release 43. Paired-end Illumina libraries 100 base pairs in length of the captured regions from a single affected mouse were produced and run in a single lane of a Genome Analyzer IIx (Illumina).

Sequence reads were mapped to the National Center for Biotechnology Information M37 assembly of the reference mouse genome with the bowtie aligner[48]. Untrimmed reads were aligned, which allowed a maximum of two sequence mismatches, and were discarded where they aligned to the genome more than once. Sequence variants were identified with the SAMtools format for storing large nucleotide sequence alignments[49], and custom Perl scripts were subsequently used to identify those in exons and splice-donor–splice-acceptor sites or unknown or strain-specific variants.

Isolation of mRNA and amplification from cDNA. Total RNA was isolated with the mirVana Isolation kit (Ambion), then cDNA was prepared with the SuperScript First-Strand Synthesis System (Invitrogen) and oligo(dT) primers. Parts of *Atp11c* were amplified by PCR with AccuPrime Taq DNA Polymerase High Fidelity (Invitrogen) and the following primer sequences: 5′-GGCCCTTCTTACATTGGACA-3′ (forward) and 5′-GAAGGT CTGGCGGATAATGA-3′ (reverse). After gel purification, PCR products were sequenced on an ABI 3730 Sequencer at the Australian Cancer Research Foundation Biomelecular Resource Facility (John Curtin School of Medical Research, Australian National University) according to the manufacturer's protocol (Applied Biosystems).

Flow cytometry and cell sorting. Cell suspensions were prepared and then counted by trypan blue exclusion, and equal number of cells were separated into aliquots in 96-well round-bottomed plates. Cells were then incubated with a primary antibody 'cocktail' containing the appropriate combination of antibodies, each diluted to its optimal concentration in flow cytometry buffer (PBS containing 2% (vol/vol) bovine serum and 0.1% (wt/vol) NaN_3), and were incubated for 30 min at 4 °C in the dark. Samples were washed and resuspended in flow cytometry buffer and were analyzed with an LSR II or LSR Fortessa (BD Biosciences).

For intracellular staining, cells were fixed and made permeable with the FoxP3 Staining kit (eBioscience). The surfaces of 1×10^6 to 2×10^6 cells were stained, and cells were washed once with flow cytometry buffer, followed by resuspension of the pelleted cells for 30 min in 50 µl Fixation/Permeabilization solution. After one wash with 1× Permeabilization buffer, cells were incubated with the appropriately conjugated antibodies to intracellular molecules. After a final wash step once with the Permeabilization buffer and once with flow cytometry buffer, cells were resuspended in flow cytometry buffer and analyzed on an LSR II (BD).

Cells were sorted by staining of single-cell suspensions from the bone marrow of mutant and control mice with the appropriate conjugated antibodies in sterile flow cytometry buffer. Pro-B cells were sorted on a FACSAria I or FACSAria II (BD Biosciences) and were collected in sterile RPMI medium supplemented with 10 mM HEPES, pH 7.2–7.5 (Sigma), 0.1 mM nonessential amino acid solution (Sigma), 1 mM sodium pyruvate (Sigma), 55 µM 2-mercapthoethanol (Gibro-BRL), 50 U/ml of penicillin-streptomycin (Gibro-BRL) and 10% (vol/vol) heat-inactivated FCS for culture.

For analysis or sorting, the following antibodies were used: anti-CD3 (145-2C11), anti-CD4 (RM4-5), anti-CD8 (53-6.7), anti-CD19 (1D3), anti-CD21-CD35 (7G6), anti-CD23 (B3B4), anti-CD25 (7D4), anti-CD43 (S7), anti-CD45.2 (104), anti-B220 (RA3-6B2), anti-Gr-1 (RB6-8C5), anti-IgM (II/41), anti-NK1.1 (PK136; all from BD); anti-CD5 (53-7.3), anti-CD8 (53-6.7), anti-CD19 (eBio1D3), anti-CD93 (AA4.1), anti-CD93 (C1qRp), anti-CD127 (A7R34), anti-c-Kit (ACK2), anti-B220 (RA3-6B2), anti-IgD (11-26), anti-IgM (II/41), anti-Flt3 (A2F10), anti-Ter119 (TER-119; all from eBiosciences); anti-CD3 (17A2), anti-CD21-CD35 (7E9), anti-CD23 (B3B4), anti-CD24 (M1/69), anti-CD43 (1B11), anti-CD45 (30-F11), anti-CD45.1 (A20), anti-BP-1 (6C3), anti-IgD (11-26c.2a), anti- Mac-1 (M1/70), anti-TCRβ (H57-597), anti-Sca-1 (D7) and annexin V (all from Biolegend); anti-CD24 (91; Southern Biotechnology); and 7-AAD and Qdot 605 streptavidin conjugate (both from Invitrogen).

For some lineage analysis (**Supplementary Fig. 5a,b**), biotin-labeled anti-CD4 (GK1.5), anti-CD5 (53-7.3), anti-CD8, anti-CD11c (HL3), anti-IgM (II/41), anti-B220 (RA3-6B2), anti-Ter119, anti-NK1.1 (PK136), anti-Ly6c (AL21), anti-Gr-1 (RB6-8C5), anti-TCRβ (H57-597), anti-TCRγδ (GL3) and anti-Mac-1 (M1/70; all from BD); and anti-CD19 (eBio1D3) and anti-IgD (11-26; both from eBioscience) were used. Qdot 605 streptavidin conjugate (Invitrogen) was used as a secondary antibody.

For other lineage analysis (**Supplementary Fig. 6a,b**), biotin-labeled anti-CD4 (GK1.5), anti-CD5 (53-7.3), anti-CD8, anti-CD11c (HL3), anti-IgM (II/41), anti-Ter119, anti-NK1.1 (PK136), anti-Ly6c (AL21), anti-Gr-1 (RB6-8C5), anti-TCRβ (H57-597), anti-TCRγδ (GL3) and anti-Mac-1 (M1/70; all from BD) were used. Qdot 605 streptavidin conjugate (Invitrogen) was used as a secondary antibody.

Generation of bone marrow chimeras. Bone marrow was extracted from donor mice by pressurized flow of sterile tissue culture medium through dissected femurs and tibias. Extracted cells were filtered and resuspended in sterile tissue culture medium. *Rag1*$^{-/-}$ recipient mice were irradiated with a single dose of 450 rads before being intravenously injected with 200 µl of 2×10^6 bone marrow donor cells per recipient mouse. After reconstitution of the hematopoietic system, lymphoid tissues were collected from the recipient mice and single-cell suspensions were prepared for analysis on an LSR II (BD Biosciences).

Cell culture. Purified pro-B cells from bone marrow were counted and then were seeded at a density of 5×10^4 to 6×10^4 cells per well onto 96-well flat-bottomed plates in sterile RPMI medium supplemented with 10 mM HEPES, pH 7.2–7.5 (Sigma), 0.1 mM nonessential amino acid solution (Sigma), 1 mM sodium pyruvate (Sigma), 55 µM 2-mercapthoethanol (Gibro-BRL), 50 U/ml of penicillin-streptomycin (Gibro-BRL) and 10% (vol/vol) heat-inactivated FCS and were incubated for up to 7 d at 37 °C and 5% CO_2 in the presence of IL-7 (25 ng/ml; R&D Systems). During culture and at the end of cultivation, cells were counted by trypan blue exclusion, then were stained with the appropriate antibodies to cell surface markers and analyzed on an LSR II (BD Biosciences).

Annexin V staining. Bone marrow and spleen cells from mutant and control mice were isolated and then were counted by trypan blue exclusion. Equal

doi:10.1038/ni.2011

numbers of cells from mutant and wild-type were allowed 'rest' for 2 h in tissue culture medium at 37 °C and 5% CO_2. Cells were then stained with the appropriate antibodies as detailed above and were washed once with flow cytometry buffer and once with Annexin V Binding Buffer (Biolegend). Cells were stained for 15 min at 20 °C with annexin V and 7-AAD in Annexin V Binding Buffer and were washed and resuspended in Annexin V Binding Buffer and analyzed on an LSR II (BD Biosciences).

Flippase assay. Flippase activity was assessed in mutant and wild-type bone marrow, spleen and thymic cells with NBD-PS (1-oleoyl-2-{6-[(7-nitro-2-1,3-benzoxadiazol-4-yl)amino]hexanoyl}-sn-glycero-3-phosphoserine (ammonium salt); Avanti Polar Lipids) as reported[50] with the following changes. For equal staining conditions for wild-type and mutant cells, equal numbers of $CD45.1^+$ wild-type cells and $CD45.2^+$ mutant cells were mixed in one tube and washed with Hank's balanced-salt solution, pH 6.0 (Gibco), prewarmed to 37 °C and supplemented with 5.5 mM D-glucose and 20 mM HEPES, pH 7.2–7.5 (solution 1). Cells were then incubated for the appropriate time at 37 °C with 5 μM NBD-PS in 200 μl solution 1. To stop the flipping in NBD-PS cells and to remove the unbound NBD-PS from the cell surface, cells were immediately placed on ice and then were incubated for 5 min with ice-cold solution 1 supplemented with 1% (wt/vol) lipid-free BSA. After 5 min, cells were spun down and washed twice in ice-cold solution 1. Cells were then transferred to 96-well plates and stained with fluorescence-labeled antibodies according to standard protocols and were analyzed on an LSR II or LSR Fortessa (BD Biosciences).

ATP11C homology model. A profile-based alignment was generated with hidden Markov models as provided by the HHPred server for homology detection and structure prediction (Bioinformatics Toolkit of the Max Planck Institute for Developmental Biology). The server identified the sarcoplasmic reticulum Ca^{2+}-ATPase (Protein Data Bank accession code, 1wpg) as the closest relative with a known structure. On the basis of the alignment, the homology model was computed with MODELLER as provided by the server.

Statistical analysis. A two-tailed Student's *t*-test and GraphPad Prism 5 (GraphPad Software) were used for statistical analysis; *P* values of less than 0.05 were considered significant.

45. Nelms, K.A. & Goodnow, C.C. Genome-wide ENU mutagenesis to reveal immune regulators. *Immunity* **15**, 409–418 (2001).
46. Mombaerts, P. *et al.* RAG-1-deficient mice have no mature B and T lymphocytes. *Cell* **68**, 869–877 (1992).
47. Randall, K.L. *et al.* Dock8 mutations cripple B cell immunological synapses, germinal centers and long-lived antibody production. *Nat. Immunol.* **10**, 1283–1291 (2009).
48. Langmead, B., Trapnell, C., Pop, M. & Salzberg, S.L. Ultrafast and memory-efficient alignment of short DNA sequences to the human genome. *Genome Biol.* **10**, R25 (2009).
49. Li, H. *et al.* The Sequence Alignment/Map format and SAMtools. *Bioinformatics* **25**, 2078–2079 (2009).
50. Hanada, K. & Pagano, R.E. A Chinese hamster ovary cell mutant defective in the non-endocytic uptake of fluorescent analogs of phosphatidylserine: isolation using a cytosol acidification protocol. *J. Cell Biol.* **128**, 793–804 (1995).